Fe-incorporated Cobalt-based Metal-organic Framework Ultrathin Nanosheets for Electrocatalytic Oxygen Evolution

Ming Zhao, Taolian Guo, Wei Qian, Zhe Wang, Xin Zhao, Lili Wen, Daping He

PII: S1385-8947(21)01640-5
DOI: https://doi.org/10.1016/j.cej.2021.130055
Reference: CEJ 130055

To appear in: *Chemical Engineering Journal*

Received Date: 16 January 2021
Revised Date: 16 April 2021
Accepted Date: 21 April 2021

Please cite this article as: M. Zhao, T. Guo, W. Qian, Z. Wang, X. Zhao, L. Wen, D. He, Fe-incorporated Cobalt-based Metal-organic Framework Ultrathin Nanosheets for Electrocatalytic Oxygen Evolution, *Chemical Engineering Journal* (2021), doi: https://doi.org/10.1016/j.cej.2021.130055

Fe-incorporated Cobalt-based Metal-organic Framework Ultrathin Nanosheets for Electrocatalytic Oxygen Evolution

Ming Zhao [a], Taolian Guo [a], Wei Qian [b], Zhe Wang [b], Xin Zhao [b], Lili Wen [a, *], Daping He [b, *]

[a] Key Laboratory of Pesticide & Chemical Biology of Ministry of Education, College of Chemistry, Central China Normal University, Wuhan 430079, China

[b] Hubei Engineering Research Center of RF-Microwave Technology and Application, Wuhan University of Technology, Wuhan 430070, China.

*E-mail: wenlili@mail.ccnu.edu.cn (L. L. Wen); hedaping@whut.edu.cn (D. P. He).

ABSTRACT: Rationally designing highly active electrocatalysts for the oxygen evolution reaction (OER) is exceedingly essential for ecologically sustainable development, but is still a principal research challenge due to the sluggish four-electron kinetics. Due to their structural diversity and ultra-high surface area, metal-organic framework (MOF) ultrathin nanosheets have expected to provide not only more accessible active sites, but also faster mass transfer and diffusion and have been realized as OER electrocatalysts. Therefore, we develop the controllable synthesis of Co-based MOF ultrathin nanosheets (NMOF-Co) incorporated with different-valence Fe ions, which are used as a high-performance electrocatalyst via a post-synthetic

modification method. The binary metal electrocatalyst demonstrated more effective kinetics than the single metal electrocatalysts. By virtue, the obtained electrocatalyst with a uniform thickness of ~ 4 nm (defined as $(Fe(II)_1Fe(III)_1)_{0.6}$/NMOF-Co) sets in at potential of only 1.56 V with small Tafel slope of 50 $mV \cdot dec^{-1}$, which is more superb than that of RuO_2 and bulk material $Fe(II)_1Fe(III)_1)_{0.6}$/Bulk-MOF-Co. The findings show that the structure of ultrathin nanosheets and the Fe incorporation are critical to the outstanding performance of MOF nanosheets for tuning the electrocatalytic activity, which is of great significance in the field of MOF electrocatalysis.

KEYWORDS: Fe-incorporated, ultrathin nanosheets, free-noble metal, metal–organic frameworks, oxygen evolution reaction.

INTRODUCTION

Due to increasing demand for global energy and the intensification of environmental protection issues, the development of renewable energy conversion techniques has received extensive attention. As far as the status is concerned, opening up alternative electrochemical storage technologies has great significance for the storage and utilization of renewable energy,[1-6] at which, OER is a crucial half-reaction at anode. The OER process involves a four-electron route under alkaline conditions, and the most recognized theory is as follows:

$$M + OH \longrightarrow M\text{-}OH + e^- \quad (1)$$

$$M\text{-}OH + OH^- \longrightarrow M\text{-}O^- + H_2O \quad (2)$$

$$M\text{-}O^- \longrightarrow M\text{-}O + e^- \quad (3)$$

$$2M\text{-}O \longrightarrow 2M + O_2 \quad (4)$$

the sluggish kinetics of OER commonly give rise to high overpotentials, extremely lowering the energy conversion efficiency of the devices.[7,8] Thus, efficient electrocatalysts are extremely demanded to promote OER efficaciously. So far, noble metal-based catalysts have been deemed to be effective oxygen electrocatalysts for OER (such as RuO_2, Rh_2O_3 and IrO_2), but their intrinsic drawbacks of shortage and high-cost seriously impede their practical applications.[9,10] For the purpose of overcoming these issues, exploring highly efficient, low-cost and non-precious-metal-containing electrocatalysts with comparable or even better electrocatalytic activity is the major task.

Recently, a large supply of studies have been devoted to searching for non-precious alternatives, involving transition metal phosphides,[11,12] and chalcogenides,[13,14] perovskite oxides[15] and MOFs.[16-18] Among them, MOFs are promising materials acted as suitable catalyst candidates because of their adjustable pore structures and large surface areas.[19-22] However, a large number of MOFs with their intrinsically low conductivity and instability in harsh electrolytes results electrocatalytic activities far from reaching the standard in practical applications. To undergo these native shortcomings, a number of researches have been devoted to exploring multiple engineering strategies, such as carbonization by annealing treatment. For example, Mu and coworkers[23-26] have carried out tremendous related researches. However, the high temperature calcination generally requests multistep synthesis procedures and high energy input and the calcination usually induces shrink/agglomeration, which would destroy the structure of MOF and decrease the explosion of active sites. Recent works have demonstrated the MOF nanosheets with ultrathin thickness have the superior electrochemical properties.[27-35] Further compared with the bulk counterparts, MOF nanosheets are expected to provide not only more accessible active sites, but also faster mass transfer and diffusion. Therefore, it's reasonable

that the miniaturization of MOF nanosheets could maximize the accessibility of active sites and is now becoming one of the most promising synthesis strategies for improved OER.[36-39] Very recently, the nanostructure of Co/Ni-MOFs[40, 41] and Fe-MOFs[42] are regarded as high-efficiency oxygen electrocatalysts as well as are explored to be stable and active for OER. What is more, many researches have verified that Fe incorporating can further increase the OER properties of Co-based MOFs with high durability.[21,43] In 2017, Shen and coworkers[44] completely reported a modular synthesis method that the Co carboxylate cluster of paddle-wheel type were immobilized in a unmatched Fe(III)-node framework, which displayed satisfactory electrochemical activity and long-term electrochemical durability for OER. In 2018, Xiao et al.[28] prepared the ultrathin Co/Ni bimetal-organic framework nanobelts (Co/Ni-MOFs) by hydrothermal process. Successfully, the Co/Ni-MOF nanobelts catalyst attained exceedingly high bifunctional catalytic activities without pyrolysis. Using solvothermal process, Xie and coworkers[18] prepared the Co/Fe-based bimetallic MOF nanosheet arrays integrated on a piece of Ni foam (MIL-53(Co-Fe)/NF), which can directly make a crucial contribution to the highly efficient electrocatalysts.

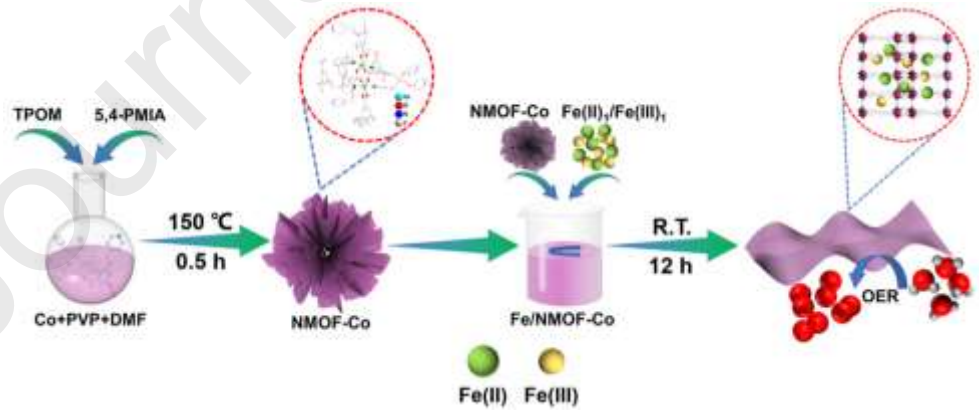

Scheme 1. Schematic illustration of the fabrication process for $(Fe(II)_1Fe(III)_1)_{0.6}$/NMOF-Co.

Drawing inspiration from the aboved researches, herein, we report the facile synthesis of $(Fe(II)_1Fe(III)_1)_x$/NMOF-Co composites for OER by introducing iron ions with different valence states into Co-based MOF ultrathin nanosheets (NMOF-Co) and show its potential application in electrocatalysis. Scheme 1 shows the synthetic process of $(Fe(II)_1Fe(III)_1)_x$/NMOF-Co (for details see Supporting Information). Experimental results demonstrate the brilliant electrocatalytic activity and stability of $(Fe(II)_1Fe(III)_1)_{0.6}$/NMOF-Co for OER after loading with XC-72 carbon particles. Furthermore, $(Fe(II)_1Fe(III)_1)_{0.6}$/NMOF-Co can be loaded on a nickel foam (NF) and achieved catalyst $(Fe(II)_1Fe(III)_1)_{0.6}$/NMOF-Co/NF exhibits enhanced OER activity with 297 mV to afford 10 mA cm^{-2} that outperforms the commercial RuO_2 catalyst.

EXPERIMENTAL AND METHOD SECTION

2.1. Synthesis of $(Fe(II)_1Fe(III)_1)_{0.6}$/NMOF-Co. $(Fe(II)_1Fe(III)_1)_{0.6}$/NMOF-Co was synthesized by a post-synthetic method in which the molar ratio of ammonium iron(II) sulfate to ferric sulfate remained as 1:1. NMOF-Co (3.5 mmol), ammonium iron(II) (1.4 mmol) sulfate and ferric sulfate (1.4 mmol) was immersed in acetonitrile (2 mL) under room temperature by stirring for 12 hours. Then the obtained mixture was washed with ethanol as well as centrifuged for 3~5 times and dried for 6 hours under vacuum. The resulting product named $(Fe(II)_1Fe(III)_1)_{0.6}$/NMOF-Co. For control, the same synthesis procedure was adopted for $(Fe(II)_1Fe(III)_1)_x$/NMOF-Co by altering molar amounts of $Fe(II)_1Fe(III)_1$ and NMOF-Co. (x is the molar ratios of $Fe(II)_1Fe(III)_1$ to NMOF-Co).

2.2. Synthesis of $(Fe(II)_1Fe(III)_1)_{0.6}$/Bulk-MOF-Co. For comparison, $(Fe(II)_1Fe(III)_1)_{0.6}$/Bulk-MOF-Co was prepared via the similar process to that of $((Fe(II)_1Fe(III)_1)_x$/NMOF-Co except that Bulk-MOF-Co was used to replace NMOF-Co nanosheets.

2.3. Electrochemical measurements.

According to the previous report,[45] the TOF of $(Fe(II)_1Fe(III)_1)_{0.6}$/NMOF-Co for OER was evaluated by the formula below:

$$TOF = n_{O2} / n_{cat} / t$$

where n_{O2} is the amount of oxygen produced (mol), n_{cat} is the amount of catalytic active centers in the catalyst (mol) and t is the electrolysis time (s).

$$TOF_{theoretical} = J \times A / (4 \times F \times m)$$

Here, J is the current density at the overpotential of 0.33 V, and A and m are the area of the electrode and the number of moles of the catalysts that deposited on the GCE, respectively. F is the Faraday constant (96485 $C \cdot mol^{-1}$). We assumed all the metal atoms contribute to the activity.

RESULTS AND DISCUSSION

3.1. Morphology and Structure Characterization. In our previous work,[46] NMOF-Co possessing flower-like morphology were successfully prepared with the assistance of polyvinylpyrrolidone (PVP) using a bottom-up method, which is distinguished from their bulk counterpart Bulk-MOF-Co (Figure S1). By changing the molar ratios of $Fe(II)_1Fe(III)_1$ to NMOF-Co, the $(Fe(II)_1Fe(III)_1)_x$/NMOF-Co with four different molar ratios can be obtained (Table S1 and Table S2). The Power X-ray diffraction (PXRD) patterns of NMOF-Co, $(Fe(II)_1Fe(III)_1)_{0.3}$/NMOF-Co, $(Fe(II)_1Fe(III)_1)_{0.6}$/NMOF-Co, $(Fe(II)_1Fe(III)_1)_{3.5}$/NMOF-Co, and $(Fe(II)_1Fe(III)_1)_{7.0}$/NMOF-Co shown well-defined and similar diffraction peaks that were in accordance with the simulated patterns in Fig. 1a and Fig. S2. It confirmed that the crystalline phase did not change after introducing Fe ions.[47] Furthermore, the simulated sample belongs to bulk material Bulk-MOF-Co while $(Fe(II)_1Fe(III)_1)_{0.6}$/NMOF-Co is two dimensional ultrathin nanosheets. The different synthesis process of Bulk-MOF-Co and $(Fe(II)_1Fe(III)_1)_{0.6}$/NMOF-Co not only determines nucleate growth of MOFs but also controls their growth direction which

causes the materials to expose different crystal planes and result in differences of diffraction peaks. The slight differences in the peak positions and intensities of the XRD patterns of the $(Fe(II)_1Fe(III)_1)_{0.6}$/NMOF-Co and simulated sample were possibly attributed to the different host-guest interactions of the flexible $(Fe(II)_1Fe(III)_1)_{0.6}$/NMOF-Co framework when Co^{2+} was partially replaced by Fe^{2+}/Fe^{3+}.[48,49] The optimized molar ratio of $(Fe(II)_1Fe(III)_1)$/NMOF-Co was 0.6:1 (Table S1). In order to obtain the most favorable activities, the linear sweep voltammetry (LSV) curves of iron ions of different valence states with diverse molar amounts of Fe(II) and Fe(III) under room temperature were recorded as shown in Fig. S3. These results suggested that molar ratios of Fe(II)/Fe(III) played a vital role in OER activity of $(Fe(II)_aFe(III)_b)_{0.6}$/NMOF-Co (a and b are defined as molar ratios of Fe(II)/Fe(III) which the optimized value is 1:1). As shown in Fig. S4, the Fourier transform infrared spectra (FT-IR) shown negligible variance compared with the untreated samples NMOF-Co. Since four $(Fe(II)_1Fe(III)_1)_x$/NMOF-Co are isostructural, only $(Fe(II)_1Fe(III)_1)_{0.6}$/NMOF-Co is discussed below.

The element chemical status of $(Fe(II)_1Fe(III)_1)_{0.6}$/NMOF-Co was investigated by X-ray photoelectron spectroscopy (XPS), as demonstrated in Fig. 1b, 1c, 1d and 1f. The survey spectrum of $(Fe(II)_1Fe(III)_1)_{0.6}$/NMOF-Co shown the presence of C, N, O, Co and Fe in Fig. 1b. The C 1s spectrum (Fig. 1c) can be deconvoluted well into four surface carbon components at 284.6 eV (nonoxygenated carbon: C-C), 285.3 eV (C-N), 286 eV (C-O) and 288 eV (carboxyl carbon: O=C-O). In the high-resolution of O 1s region, three peaks at approximately 530.95, 531.8 and 533.05 eV displayed the existence of Co-O, C=O-O and C-O, respectively (Fig. 1d). Co 2p displayed major peaks of Co $2p_{3/2}$ (781.1 eV) and Co $2p_{1/2}$ (796.8 eV), implying the existence of Co^{2+} state (Fig. 1e).[36] The high-resolution Fe 2p spectra can be fitted into six peaks from 708 eV to 735 eV in Fig. 1f, namely satellite peak (715.9 eV and 719.1 eV) and Fe $2p_{1/2}$

(Fe(II) 723.6 eV, Fe(III) 725 eV) and Fe $2p_{3/2}$ (Fe(II) 711.1 eV, Fe(III) 713.5 eV), illustrating that both ferrous and ferric irons existed in $(Fe(II)_1Fe(III)_1)_{0.6}$/NMOF-Co.[50] Inductively coupled plasma-mass spectrometry (ICP) measurements revealed that it contained 7.41% Co and 4.64% Fe, implying a 0.6:1 stoichiometry of Fe/Co in $(Fe(II)_1Fe(III)_1)_{0.6}$/NMOF-Co. The ICP results were well-consistent with the added ratios (Table S2).

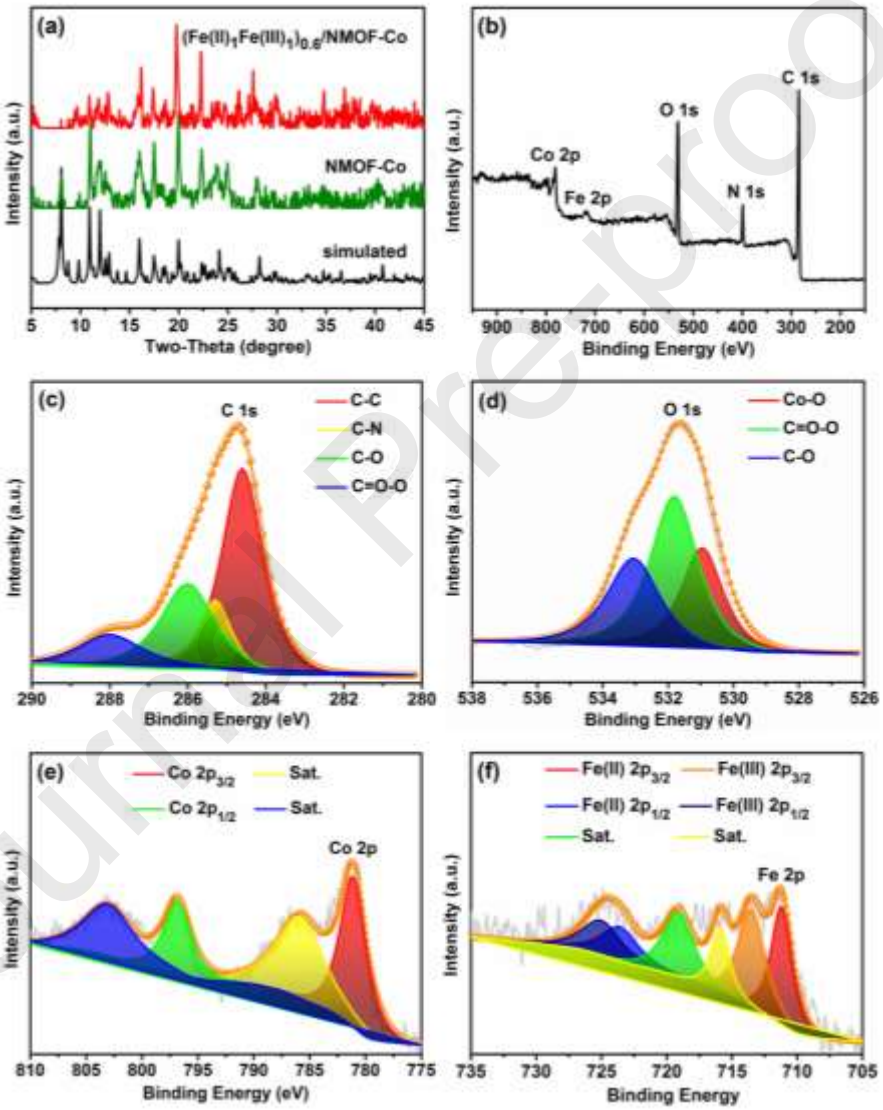

Fig. 1. (a) PXRD patterns for $Fe(II)_1Fe(III)_1)_{0.6}$/NMOF-Co and NMOF-Co. XPS spectra of (b) Survey scan, (c) C 1s, (d) O 1s, (e) Co 2p and (f) Fe 2p of $(Fe(II)_1Fe(III)_1)_{0.6}$/NMOF-Co.

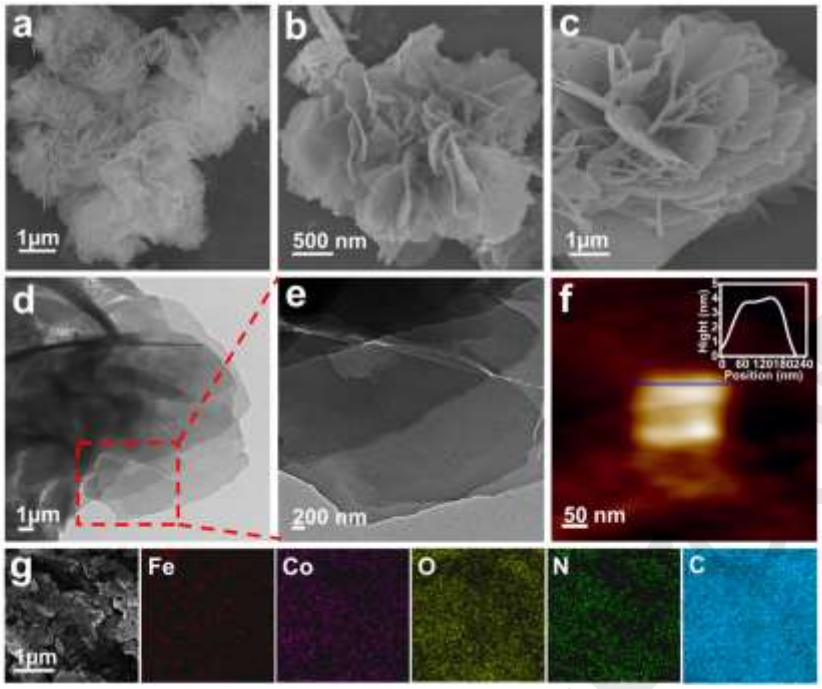

Fig. 2. (a), (b) Low and high-resolution SEM images of NMOF-Co nanosheets. (c) SEM images of $(Fe(II)_1Fe(III)_1)_{0.6}$/NMOF-Co nanosheets. Typical (d), (e) TEM image and (f) AFM image of $(Fe(II)_1Fe(III)_1)_{0.6}$/NMOF-Co nanosheets. (g) SEM-EDX elemental mapping of $(Fe(II)_1Fe(III)_1)_{0.6}$/NMOF-Co nanosheets.

The morphological properties of NMOF-Co and $(Fe(II)_1Fe(III)_1)_{0.6}$/NMOF-Co were vividly seen from Fig. 2. As shown in Fig. 2a and 2b, scanning electron microscopy (SEM) images shown that the obtained NMOF-Co was composed of numerous ultrathin nanosheets. In particular, after introducing Fe ions, $(Fe(II)_1Fe(III)_1)_x$/NMOF-Co inherited the nanosheets-stacked morphology of NMOF-Co (Fig. 2c and Fig. S1), in sharp contrast to the Bulk-MOF-Co, which exhibited irregular bulks with a wide size distribution varying from hundreds of nanometers to dozens of micrometers (Fig. S1a). Additionally, transmission electron microscopy (TEM) images (Fig. 2d and 2e) provided more insight into the structure of $(Fe(II)_1Fe(III)_1)_{0.6}$/NMOF-Co, proving the nanosheet nature of this material. Fig. 2e further

demonstrated that the as-synthesized sample presented ultrathin and translucent sheet-like morphology, which was advantageous to the transport of electrons and protons. The thickness of composite ultrathin nanosheets were determined to be ~4.0 nm by atomic force microscopy (AFM) measurement (Fig. 2f). The energy-dispersive X-ray spectrum (EDX)-mapping revealed the elements of C, N, O, Co and Fe without other impurities in MOFs and their homogeneous distribution throughout the whole construction in Fig. 2g. All abovementioned data suggested the successful synthesis of $(Fe(II)_1Fe(III)_1)_{0.6}$/NMOF-Co nanosheets.

3.2. Electrochemical Performance. The electrocatalytic OER performance of as-prepared $(Fe(II)_1Fe(III)_1)_{0.6}$/NMOF-Co were explored in alkaline condition (1M KOH electrolyte) with a standard three-electrode system, where XC-72 were modified with as-prepared catalysts by drop-casting as the working electrode to improve the conductivity. All data were obtained without iR-correction. Commercially RuO_2 was tested under the same condition for comparison. The linear sweep voltammetry curves (LSV), Tafel plots and electrochemical impedance spectroscopy (EIS) results were presented in Fig. 3. As shown in Fig. 3a, the onset potential (E_{onset}) of NMOF-Co was 1.281 V. Introducing Fe ions caused the E_{onset} much lower for $(Fe(II)_1Fe(III)_1)_{0.6}$/NMOF-Co, highlighting the positive role of Fe ions. Remarkably, the $(Fe(II)_1Fe(III)_1)_{0.6}$/NMOF-Co with two-dimensional morphology shown superior OER performance with an onset potential of only 1.267 V, much lower than that of $(Fe(II)_1Fe(III)_1)_{0.6}$/Bulk-MOF-Co (1.277 V), suggesting that the morphology of ultrathin nanosheets was beneficial for improved OER. Noticeably, the E_{onset} of $(Fe(II)_1Fe(III)_1)_{0.6}$/NMOF-Co was comparable to that of RuO_2 (1.269 V), implying its excellent OER activity. Tafel slope analysis further confirmed the fast OER kinetics of $(Fe(II)_1Fe(III)_1)_{0.6}$/NMOF-Co. As shown in Fig. 3b, the Tafel slop of $(Fe(II)_1Fe(III)_1)_{0.6}$/NMOF-Co was as low as 50 mV dec^{-1}, lower than those of NMOF-Co (144 $mV \cdot dec^{-1}$),

$(Fe(II)_1Fe(III)_1)_{0.6}$/Bulk-MOF-Co (95 mV dec^{-1}) and RuO_2 (77 mV dec^{-1}), suggesting the faster OER kinetics of $(Fe(II)_1Fe(III)_1)_{0.6}$/NMOF-Co. In addition to the E_{onset} and Tafel slope values, the current density of 10 mA cm^{-2} was another critical criterion for assessment of OER performance. As presented in Fig. 3c, the potentials of NMOF-Co, $(Fe(II)_1Fe(III)_1)_{0.6}$/Bulk-MOF-Co, $(Fe(II)_1Fe(III)_1)_{0.6}$/NMOF-Co and RuO_2 were 1.64, 1.625, 1.56 and 1.565 V, respectively. To further investigate the transfer kinetics of charge carriers, electrochemical impedance spectroscopies (EIS) was measured in 1.0 M KOH. The EIS results (Fig. 3d) shown that $(Fe(II)_1Fe(III)_1)_{0.6}$/NMOF-Co displayed a small charge transfer resistance (Rct) of 50 ohm at the overpotential of 330 mV, which was far less than that of $(Fe(II)_1Fe(III)_1)_{0.6}$/Bulk-MOF-Co (82 ohm)，$RuO_2$ (56 ohm in Fig. S8) and NMOF-Co (100 ohm). It revealed a faster electron transfer ability of $(Fe(II)_1Fe(III)_1)_{0.6}$/NMOF-Co owing to incorporation of Fe ions and ultrathin nano-structure. As depicted in Fig. 3e, the catalyst $(Fe(II)_1Fe(III)_1)_{0.6}$/NMOF-Co displayed optimal overpotential of 330 mV to reach the 10 mA cm^{-2}, showing an exceptional OER performance. Collectively, these electrochemical results undoubtedly demonstrated that both Fe ions and nanosheets morphology were favorable for enhanced OER. Such that we then optimized the content of Fe ions in NMOF-Co. Among them, the overpotential of $(Fe(II)_1Fe(III)_1)_{0.6}$/NMOF-Co was the lowest, indicating more superior OER reaction kinetics. Besides, the high activity of the NiFe-UMNs was also verified by the TOF calculated at 1.12 s^{-1}. Additionally, the long-term stability was another significant parameter to estimate electrocatalysts for applicability. The stability of $(Fe(II)_1Fe(III)_1)_{0.6}$/NMOF-Co was tested by chronopotentiometry and cyclic voltammetry (CV). As shown in Fig. 3f, after CV between 1.2 and 1.6 V for 1000 cycles, $(Fe(II)_1Fe(III)_1)_{0.6}$/NMOF- Co merely displayed mild degradation, demonstrating its preferable durability during the electrocatalytic process in this work.

Moreover, the i-t curves at 10 mA cm^{-2} retained its electrochemical activity for 10000 s (inset of Fig. 3f). To further confirm the possible variance of the chemical composition on the surfaces and the electronic states of $(Fe(II)_1Fe(III)_1)_{0.6}$/NMOF-Co electrocatalyst, XPS measurements of this sample after the OER tests were also done in Fig. S5. After OER performance, the signals of Co 2p (Fig. S5a) and Fe(II) shifted to higher binding energies, while the signals of Fe(III) shifted to lower binding energies in the Fe 2p spectrum (Fig. S5b), indicating a partial electron transfer between different metal ions. However, the molar ratio of iron ions with disparate-valence states was almost unvaried in $(Fe(II)_1Fe(III)_1)_{0.6}$/NMOF-Co (1.1:1). The aboved data shown that two valence irons at work. It revealed that the addition of different-valence Fe species can change the ability of the material to accept electrons during OER tests, which influenced the coupling effect between Co and Fe in $(Fe(II)_1Fe(III)_1)_{0.6}$/NMOF-Co and thus promoted the OER kinetics synergistically.[31,51,52] In order to understand the improved OER performance of $(Fe(II)_1Fe(III)_1)_{0.6}$/NMOF-Co in comparison to that of $(Fe(II)_1Fe(III)_1)_{0.6}$/Bulk-MOF-Co, NMOF-Co and $(Fe(II)_1Fe(III)_1)_x$/NMOF-Co , their electrochemically active surface areas (ECSAs) were conducted from the electrochemical double-layer capacitance (Cdl) via collecting cyclic voltammograms of 1.0 to 1.24 V vs. RHE (Fig. 4a and 4b). As shown in Fig. 4a, the CV curves of different catalysts at a same rate of 40 mV s^{-1} and the $(Fe(II)_1Fe(III)_1)_{0.6}$/NMOF-Co at miscellaneous rates varying from 20 to 80 mV s^{-1} (Fig. 4b and Fig. S6). The Cdl results suggested that composited material $(Fe(II)_1Fe(III)_1)_{0.6}$/NMOF-Co had larger ECSA than that of $(Fe(II)_1Fe(III)_1)_{0.6}$/Bulk-MOF-Co when used as alkaline (1M KOH) OER electrocatalysts. As shown in Fig. 4c, $(Fe(II)_1Fe(III)_1)_{0.6}$/NMOF-Co (11.75 mF cm^{-2}) exhibited a larger Cdl than that of $(Fe(II)_1Fe(III)_1)_{0.6}$/Bulk-MOF-Co (2.24 mF cm^{-2}), $(Fe(II)_1Fe(III)_1)_{0.3}$/NMOF-Co (7.35 mF cm^{-2}),

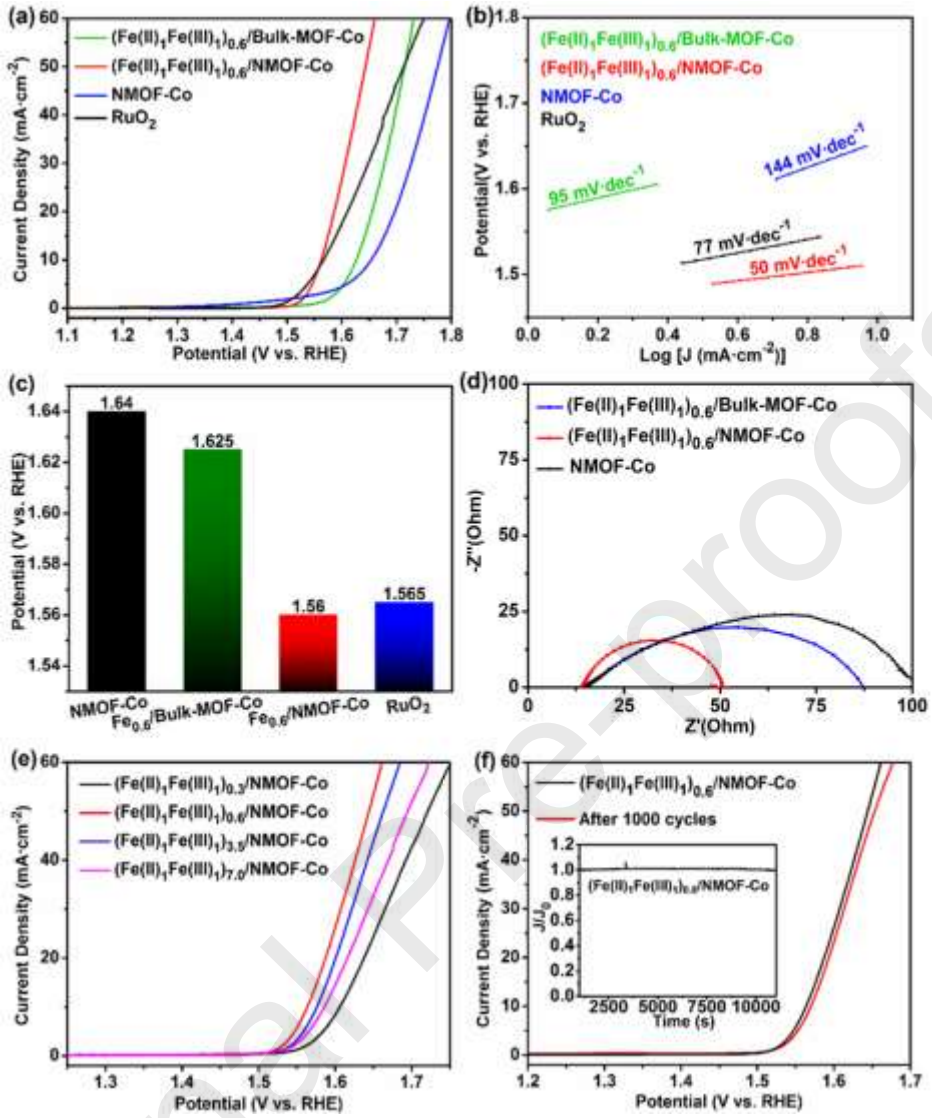

Fig. 3. (a) LSV curves and (b) Tafel plots of $(Fe(II)_1Fe(III)_1)_{0.6}$/Bulk-MOF-Co, $(Fe(II)_1Fe(III)_1)_{0.6}$/NMOF-Co, NMOF-Co and RuO_2 electrocatalysts in the OER in 1M KOH. (c) Comparison of the overpotential at current density of 10 mA cm^{-2}. (d) Electrochemical impedance spectrum of $(Fe(II)_1Fe(III)_1)_{0.6}$/Bulk-MOF-Co, $(Fe(II)_1Fe(III)_1)_{0.6}$/NMOF-Co and NMOF-Co catalysts. (e) LSV curves of $(Fe(II)_1Fe(III)_1)_x$/NMOF-Co with different molar ratios of Fe/Co. (f) Polarization curves of $(Fe(II)_1Fe(III)_1)_{0.6}$/NMOF-Co after 0 and 1000 CV cycles (inset: OER time-dependent stability of $(Fe(II)_1Fe(III)_1)_{0.6}$/NMOF-Co by chronoamperometric response).

$(Fe(II)_1Fe(III)_1)_{3.5}$/NMOF-Co (10.9 mF cm^{-2}), $(Fe(II)_1Fe(III)_1)_{7.0}$/NMOF-Co (7.37 mF cm^{-2}) and NMOF-Co (1.17 mF cm^{-2}). The results suggested that the $(Fe(II)_1Fe(III)_1)_{0.6}$/NMOF-Co were not only highly active but also stable electrocatalysts for OER, that further confirming the excellent OER performance of the composite catalysts. The catalyst NMOF-Co composited with $Fe(II)_1Fe(III)_1$ performed optimally at the molar ratio of 1:0.6, while either lower or higher dopant ratio led to decrease OER activity. Therefore, the positive effect of Fe into $(Fe(II)_1Fe(III)_1)_x$/NMOF-Co for OER was confirmed, and the possible mechanism could be explained that iron ions were active sites and cobalt cations contributed to formulating these active sites in catalysts for oxygen evolution.[53-55]

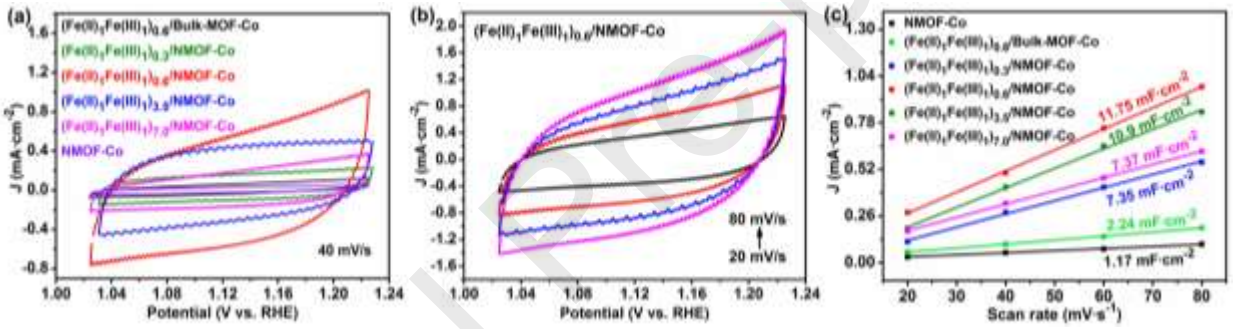

Fig. 4. (a) Cyclic voltammograms collected at same scan rate (40 mV s^{-1}) for $(Fe(II)_1Fe(III)_1)_x$/NMOF-Co, (b) Cyclic voltammograms collected at various scan rates (20, 40, 60 and 80 mV s^{-1}) for $(Fe(II)_1Fe(III)_1)_{0.6}$/NMOF-Co, (c) The double-layer capacitance (Cdl) of $(Fe(II)_1Fe(III)_1)_x$/NMOF-Co.

It should be noted that MOF ultrathin nanosheets electrocatalysts grown on conducting materials such as carbon substrate, nickel foam and copper foam have remarkable electrochemical performance due to rapid charge transport and high percentages of active sites.[21,56-62] Inspired by the abovementioned strategies, we fabricated the work-electrodes by compositing $(Fe(II)_1Fe(III)_1)_{0.6}$/NMOF-Co with Ni foam ($(Fe(II)_1Fe(III)_1)_{0.6}$/NMOF-Co/NF). As

expected, the OER activities of $(Fe(II)_1Fe(III)_1)_{0.6}$/NMOF-Co/NF were obviously enhanced, implying a lower overpotential of 297 mV at 10 mA cm^{-2} (Fig. S7a) and the corresponding Tafel slopes (Fig. S7b) of $(Fe(II)_1Fe(III)_1)_{0.6}$/NMOF-Co/NF, $(Fe(II)_1Fe(III)_1)_{0.6}$/Bulk-MOF-Co/NF, NMOF-Co/NF, RuO_2/NF and NF were 55, 81, 85, 70 and 119 mV dec^{-1} respectively. Ultimately, several recently reported highly active electrocatalysts for OER were summarized in Table S3. The hierarchical ultrathin nanosheets in $(Fe(II)_1Fe(III)_1)_x$/NMOF-Co not only provided electron transport pathway but also accelerated electron transfer capabilities, thus resulting the brilliant OER performance in alkaline medium. Moreover, the unique nanostructure also contributed to facilitate more efficacious contact between reactants and catalysts as well as promote mass transfer efficiency.

CONCLUSION

In summary, we successfully prepared a series of $Fe(II)_1Fe(III)_1)_x$/NMOF-Co with controllable molar ratios as high-performance OER electrocatalysts via a post-synthetic strategy. By compositing the optimized electrocatalyst $(Fe(II)_1Fe(III)_1)_{0.6}$/NMOF-Co with XC-72, an potential of 1.56 V vs. RHE with Tafel slope of 50 mV dec^{-1} were achieved for OER in 1M KOH. The intrinsic activity of the obtained electrocatalyst was also investigated by measuring the turnover frequency (TOF = 1.12 s^{-1}). It is concluded that the MOF ultrathin nanosheets of $(Fe(II)_1Fe(III)_1)_x$/NMOF-Co not only facilitated more efficient electron transfer but also endowed the material with more active sites for efficacious contact between the reactants and catalysts. It is also worth noting that, by adjusting the molar ratios of $Fe(II)_1Fe(III)_1$ to NMOF-Co, we can modulate the activity and stability in a controllable manner. This work opens up a new route for reasonable design and preparation of high-performance nonprecious-metal catalysts for electrocatalysis.

AUTHOR INFORMATION

Corresponding Author

Lili Wen - Key Laboratory of Pesticide & Chemical Biology of Ministry of Education, College of Chemistry, Central China Normal University, Wuhan 430079, China;

E-mail: wenlili@mail.ccnu.edu.cn

Daping He - Hubei Engineering Research Center of RF-Microwave Technology and Application, Wuhan University of Technology, Wuhan 430070, China;

E-mail: hedaping@whut.edu.cn

Authors

Ming Zhao - Key Laboratory of Pesticide & Chemical Biology of Ministry of Education, College of Chemistry, Central China Normal University, Wuhan 430079, China

Taolian Guo - Key Laboratory of Pesticide & Chemical Biology of Ministry of Education, College of Chemistry, Central China Normal University, Wuhan 430079, China

Wei Qian - Hubei Engineering Research Center of RF-Microwave Technology and Application, Wuhan University of Technology, Wuhan 430070, China.

Zhe Wang - Hubei Engineering Research Center of RF-Microwave Technology and Application, Wuhan University of Technology, Wuhan 430070, China.

Xin Zhao - Hubei Engineering Research Center of RF-Microwave Technology and Application, Wuhan University of Technology, Wuhan 430070, China.

Author Contributions

The manuscript was written through the contributions of all authors. All authors have approved the final version of the manuscript.

Notes

The authors declare no competing financial interest.

ACKNOWLEDGMENT

This work was financially supported by the National Natural Science Foundation of China (Nos. 21771072 and 21371065). This project is also partially funded by the 111 Project B17019.

REFERENCES

[1] Z. W. Seh, J. Kibsgaard, C. F. Dickens, I. Chorkendorff, J. K. Nørskov, T. F. Jaramillo, Combining theory and experiment in electrocatalysis: insights into materials design, Science 355 (2017) eaad4998.

[2] H. Jin, C. Guo, X. Liu, J. Liu, A. Vasileff, Y. Jiao, Y. Zheng, S. Qiao, Emerging two-dimensional nanomaterials for electrocatalysis, Chem. Rev. 118 (2018) 6337-6408.

[3] Y. Jiao, Y. Zheng, M. Jaroniec, S. Z. Qiao, Design of electrocatalysts for oxygen-and hydrogen-involving energy conversion reactions, Chem. Soc. Rev. 44 (2015) 2060-2086.

[4] S. Park, Y. Shao, J. Liu, Y. Wang, Oxygen electrocatalysts for water electrolyzers and reversible fuel cells: status and perspective, Energy Environ. Sci. 5 (2012) 9331-9344.

[5] X. F. Lu, L. Yu, X. Lou, Highly crystalline Ni-doped FeP/carbon hollow nanorods as all-pH efficient and durable hydrogen evolving electrocatalysts, Sci. Adv. 5 (2019) eaav6009.

[6] T. He, S. Chen, B. Ni, Y. Gong, Z. Wu, L. Song, L. Gu, W. Hu, X. Wang, Zirconium-porphyrin-based metal-organic framework hollow nanotubes for immobilization of noble-metal single atoms, Angew. Chem. Int. Ed. 57 (2018) 3493-3498.

[7] C. C. L. McCrory, S. Jung, J. C. Jung, T. F. Jaramillo, Benchmarking heterogeneous electrocatalysts for the oxygen evolution reaction, J. Am. Chem. Soc. (135) 2013 16977-16987.

[8] K. J. May, C. E. Carlton, K. A. Stoerzinger, M. Risch, J. Suntivich, Y. Lee, A. Grimaud, Y. Shao-Horn, Influence of oxygen evolution during water oxidation on the surface of perovskite oxide catalysts, J. Phys. Chem. Lett. 3 (2012) 3264-3270.

[9] H. B. Gray, Powering the planet with solar fuel, Nat. Chem. 1 (2009) 7.

[10] Y. Yang, H. Fei, G. Ruan, J. M. Tour, Porous cobalt-based thin film as a bifunctional catalyst for hydrogen generation and oxygen generation, Adv. Mater. 27 (2015) 3175-3180.

[11] Y. Zhao, X. Jia, G. Chen, L. Shang, G. I. N. Waterhouse, L. Wu, C. Tung, D. O'Hare, T. Zhang, Ultrafine NiO nanosheets stabilized by TiO from monolayer NiTi-LDH precursors: an active water oxidation electrocatalyst, J. Am. Chem. Soc. 138 (2016) 6517-6524.

[12] P. Jiang, Q. Liu, Y. Liang, J. Tian, A. M. Asiri, X. Sun, A cost-effective 3D hydrogen evolution cathode with high catalytic activity: FeP nanowire array as the active phase, Angew. Chem, Int. Ed. 53 (2014) 12855-12859.

[13] Y. P. Zhu, T. Y. Ma, M. Jaroniec, S. Z. Qiao, Self-templating synthesis of hollow Co_3O_4 microtube arrays for highly efficient water electrolysis, Angew. Chem. Int. Ed. 56 (2017) 1324-1328.

[14] X. H. Wang, Y. Ling, B. L. Li, X. L. Li, G. Chen, B. X. Tao, Li, J. L. Li, B. N. H. Q. Luo, Asymmetric electrodes with a transition metal disulfide heterostructure and amorphous

bimetallic hydroxide for effective alkaline water electrolysis, J. Mater. Chem. A. 7 (2019) 2895-2900.

[15] J. Suntivich, K. J. May, H. A. Gasteiger, J. B. Goodenough, Y. Shao-Horn, A perovskite oxide optimized for oxygen evolution catalysis from molecular orbital principles, Science 334 (2011) 1383-1385.

[16] F. Yang, P. Zhao, X. Hua, W. Luo, G. Cheng, W. Xing, S. Chen, A cobalt-based hybrid electrocatalyst derived from carbon nanotube inserted metal-organic framework for efficient watersplitting, J. Mater. Chem. A 4 (2016) 16057-16063.

[17] J. Huang, Y. Li, R. K. Huang, C. T. He, L. Gong, Q. Hu, L. Wang, Y. T. Xu, X. Y. Tian, S. Y. Liu, Z. M. Ye, F. Wang, D. D. Zhou, W. X. Zhang, J. P. Zhang, Electrochemical exfoliation of pillared-layer metal-organic framework for boosting the oxygen evolution reaction, Angew. Chem. Int. Ed. 57 (2018) 4632-4636.

[18] M. Xie, Y. Ma, D. Lin, C. Xu, F. W. Xie, Zeng. Bimetal-organic framework MIL-53(Co-Fe): an efficient and robust electrocatalyst for the oxygen evolution reaction, Nanoscale 12 (2020) 67-71.

[19] H. Kim, S. Yang, S. R. Rao, S. Narayanan, E. A. Kapustin, H. Furukawa, A. S. Umans, O. M. Yaghi, E. N. Wang, Water harvesting from air with metal-organic frameworks powered by natural sunlight, Science 356 (2017) 430-434.

[20] H. Furukawa, K. E. Cordova, M. O'Keeffe, O. M. Yaghi, The chemistry and applications of metal-organic frameworks. Science 341 (2013) 974-+.

[21] J. Duan, S. Chen, C. Zhao, Ultrathin metal-organic framework array for efficient electrocatalytic water splitting, Nat. Commun. 8 (2017) 15341.

[22] W. Chen, Y. Zhang, G. Chen, R. Huang, Y. Zhou, Y. Wu, Y. Hu, K. Ostrikov, Mesoporous cobalt-iron-organic frameworks: plasma-enhanced oxygen evolution electrocatalyst, J. Mater. Chem. A. 7 (2019) 3090-3100.

[23] R. Chen, Y. Tan, Z. Zhang, Z. Lei, W. Wu, N. Cheng, S. Mu, Hydrazine hydrate induced two-dimensional porous Co^{3+} enriched Co_3O_4 nanosheets for enhanced water oxidation catalysis, ACS Sustain Chem. Eng. 8 (2020) 9813-9821.

[24] Q. Liang, H. Jin, Z. Wang, Y. Xiong, S. Yuan, X. Zeng, D. He, S. Mu, Metal-organic frameworks derived reverse-encapsulation Co-NC@Mo_2C complex for efficient overall water splitting, Nano Energy 57 (2019) 746-752.

[25] I. S. Amiinu, X. Liu, Z. Pu, W. Li, Q. Li, J. Zhang, H. Tang, H. Zhang, S. Mu, From 3D ZIF nanocrystals to Co-N-x/C nanorod array electrocatalysts for ORR, OER, and Zn-Air batteries, Adv. Funct. Mater. 28 (2018) 1704638.

[26] C. G. Read, J. F. Callejas, C. F. Holder, R. E. Schaak, General strategy for the synthesis of transition metal phosphide films for electrocatalytic hydrogen and oxygen evolution, ACS Appl. Mater. Interfaces 8 (2016) 12798-12803.

[27] C. Tan, X. Cao, X. Wu, Q. He, J. Yang, X. Zhang, J. Chen, W. Zhao, S. Han, G. Nam, M. H. Sindoro, Zhang Recent advances in ultrathin two-dimensional nanomaterials, Chem. Rev. 117 (2017) 6225-6331.

[28] X. Xiao, Q. Li, X. Yuan, Y. Xu, M. Zheng, H. Pang, Ultrathin nanobelts as an excellent bifunctional oxygen catalyst: insight into the subtle changes in structure and synergistic effects of bimetallic metal-organic framework, Small Methods 2 (2018) 1800240.

[29] B. Wurster, D. Grumelli, D. Hötger, R. Gutzler, K. Kern, Driving the oxygen evolution reaction by nonlinear cooperativity in bimetallic coordination catalysts, J. Am. Chem. Soc. 138 (2016) 3623-3626.

[30] L. Wang, Y. Wu, R. Cao, L. Ren, M. Chen, X. Feng, J. Zhou, B. Wang, Fe/Ni metal-organic frameworks and their binder-free thin films for efficient oxygen evolution with low overpotential, ACS Appl. Mater. Interfaces 8 (2016) 16736-16743.

[31] S. Zhao, Y. Wang, J. Dong, C. He, H. Yin, P. An, K. Zhao, X. Zhang, C. Gao, L. Zhang, J. Lv, J. Wang, J. Zhang, A. M. Khattak, N. A. Khan, Z. Wei, J. Zhang, S. Liu, H. Zhao, Z. Tang, Ultrathin metal-organic framework nanosheets for electrocatalytic oxygen evolution, Nat. Energy 1 (2016) 1-10.

[32] L. Zhao, B. Dong, Li, S.; Zhou, L.; Lai, L.; Wang, Z.; Zhao, S.; Han, M.; Gao, K.; Lu, M.; Xie, X.; Chen, B.; Liu, Z.; Wang, X.; Zhang, H.; Li, H.; Liu, J.; Zhang, H.; Huang, X.; Huang, W. Interdiffusion reaction-assisted hybridization of two-dimensional metal-organic frameworks and $Ti_3C_2T_x$ nanosheets for electrocatalytic oxygen evolution, ACS Nano 11 (2017) 5800-5807.

[33] F. Sun, G. Wang, Y. Ding, C. Wang, B. Yuan, Y. Lin, NiFe-based metal-organic framework nanosheets directly supported on nickel foam acting as robust electrodes for electrochemical oxygen evolution reaction, Adv. Energy Mater. 8 (2018) 1800584.

[34] D. Senthil Raja, X. Chuah, S. Lu, In situ grown bimetallic MOF-based composite as highly efficient bifunctional electrocatalyst for overall water splitting with ultrastability at high current densities, Adv. Energy Mater. 8 (2018) 1801065.

[35] K. Rui, G. Zhao, Y. Chen, Y. Lin, Q. Zhou, J. Chen, J. Zhu, W. Sun, W. Huang, S. X. Dou, Hybrid 2D dual-metal-organic frameworks for enhanced water oxidation catalysis, Adv. Funct. Mater. 28 (2018) 1801554.

[36] B. Yao, L. Huang, J. Zhang, X. Gao, J. Wu, Y. Cheng, X. Xiao, B. Wang, Y. Li, J. Zhou, Flexible transparent molybdenum trioxide nanopaper for energy storage, Adv. Mater. 28 (2016) 6353-6358.

[37] T. Guo, C. Wang, N. Zhang, Zhang, Chen, T. Y. X. Xing, Z. Lu, Wen, L. Fabrication of homogeneous non-noble metal nanoparticles within metal-organic framework nanosheets for catalytic reduction of 4-nitrophenol, Cryst. Growth Des. 20 (2020) 6217-6225.

[38] T. Sun, L. Xu, D. Wang, Y. Li, Metal organic frameworks derived single atom catalysts for electrocatalytic energy conversion, Nano Research 12 (2019) 2067–2080.

[39] T. J. Wang, X. Liu, Y. Li, F. Li, Z. Deng, Y. Chen, Ultrasonication-assisted and gram-scale synthesis of Co-LDH nanosheet aggregates for oxygen evolution reaction, Nano Research 13 (2019) 79–85

[40] X. Zhang, W. Sun, H. Du, R. Kong, F. A Qu, Co-MOF nanosheet array as a high-performance electrocatalyst for the oxygen evolution reaction in alkaline electrolytes, Inorg. Chem. Front. 5 (2018) 344-347.

[41] E. A. Flügel, V. W. Lau, H. Schlomberg, R. Glaum, B. V. Lotsch, Homonuclear Mixed-valent cobalt imidazolate framework for oxygen-evolution electrocatalysis, Chem. Eur. J. 22 (2016) 3676-3680.

[42] P. Du, R. Eisenberg, Catalysts made of earth-abundant elements (Co, Ni, Fe) for water splitting: recent progress and future challenges, Energy Environ. Sci. 5 (2012) 6012-6621.

[43] M. B. Stevens, L. J. Enman, E. H. Korkus, J. Zaffran, C. D. M. Trang, J. Asbury, M. G. Kast, M. C. Toroker, Shannon W. Boettcher, Ternary Ni-Co-Fe oxyhydroxide oxygen evolution catalysts: intrinsic activity trends, electrical conductivity, and electronic band structure, Nano Research 12 (2019) 2288–2295.

[44] J. Shen, P. Liao, D. Zhou, C. He, J. Wu, W. Zhang, J. Zhang, X. Chen, Modular and stepwise synthesis of a hybrid metal-organic framework for efficient electrocatalytic oxygen evolution, J. Am. Chem. Soc. 139 (2017) 1778-1781.

[45] J. Xie, X. Zhang, H. Zhang, J. Zhang, S. Li, R. Wang, B. Pan, Y. Xie, Intralayered ostwald ripening to ultrathin nanomesh catalyst with robust oxygen-evolving performance[J]. Adv. Mater. 29 (2017) 1604765.

[46] J. Duan, R. Yan, L. Qin, Y. Wang, L. Wen, S. Cheng, H. Xu, P. Feng, Highly selective gaseous and liquid-phase separation over a novel cobalt(II) metal-organic framework, ACS Appl. Mater. Interfaces 10 (2018) 23009-23017.

[47] R. Yan, Y. Zhao, H. Yang, X. Kang, C. Wang, L. Wen, Z. Lu, Ultrasmall Au nanoparticles embedded in 2D mixed-ligand metal-organic framework nanosheets exhibiting highly efficient and size-selective catalysis, Adv. Funct. Mater. 28 (2018) 1802021.

[48] O. Shekhah, H. Wang, D. Zacher, R. A. Fischer, C. Wöll, Growth Mechanism of Metal-Organic Frameworks: Insights into the nucleation by employing a step-by-step route, Angew. Chem. Int. Ed. 48 (2009) 5038-5041.

[49] T. Ling, M. Jaroniec, S. Z. Qiao, Recent progress in engineering the atomic and electronic structure of electrocatalysts via cation exchange reactions, Adv. Mater. 32 (2020) 2001866.

[50] Z. Wang, H. Jin, T. Meng, K. Liao, W. Meng, J. Yang, D. He, Y. Xiong, S. Mu, Fe, Cu-coordinated ZIF-derived carbon framework for efficient oxygen reduction reaction and zinc-air batteries, Adv. Funct. Mater. 28 (2018) 1802596.

[51] G. Hai, X. Jia, K. Zhang, X. Liu, Z. Wu, G. Wang, High-performance oxygen evolution catalyst using two-dimensional ultrathin metal-organic frameworks nanosheets, Nano Energy 44 (2018) 345-352.

[52] G. Férey, F. Millange, M. Morcrette, C. Serre, M. Doublet, J. Grenèche, J. Tarascon, Mixed-valence Li/Fe-based metal-organic frameworks with both reversible redox and sorption properties, Angew. Chem. Int. Ed. 46 (2007) 3259-3263.

[53] B. You, Y. Zhang, P. Yin, D. Jiang, Y. Sun, Universal molecular-confined synthesis of interconnected porous metal oxides-N-C frameworks for electrocatalytic water splitting, Nano Energy 48 (2018) 600-606.

[54] B. You, N. Jiang, Y. Sun, Morphology–activity correlation in hydrogen evolution catalyzed by cobalt sulfides, Inorg. Chem. Front. 3 (2016) 279-285.

[55] B. You, Y. Sun, Hierarchically porous nickel sulfide multifunctional superstructures, Adv. Energy Mater. 6 (2016) 1502333.

[56] X. Yan, L. Tian, M. He, X. Chen, Three-dimensional crystalline/amorphous Co/Co_3O_4 core/shell nanosheets as efficient electrocatalysts for the hydrogen evolution reaction, Nano Lett. 15 (2015) 6015-6021.

[57] J. Feng, J. Wu, Y. Tong, G. Li, Efficient hydrogen evolution on Cu nanodots-decorated Ni_3S_2 nanotubes by optimizing atomic hydrogen adsorption and desorption, J. Am. Chem. Soc. 140 (2018) 610-617.

[58] G. Chen, T. Wang, J. Zhang, P. Liu, H. Sun, X. Zhuang, M. Chen, X. Feng, Accelerated hydrogen evolution kinetics on NiFe-layered double hydroxide electrocatalysts by tailoring water dissociation active sites, Adv. Mater. 30 (2018) 1706279.

[59] T. Liu, P. Diao, Nickel foam supported Cr-doped $NiCo_2O_4$ /FeOOH nanoneedle arrays as a high-performance bifunctional electrocatalyst for overall water splitting, Nano Research 13 (2020) 3299-3309.

[60] Y. Q. Feng, X. Wang, J. F. Huang, P. P. Dong, J. Jing, J. Li, L. Y. Cao, L. L. Feng, P. Jing, C. R. Ru, Decorating CoNi layered double hydroxides nanosheet arrays with fullerene quantum dot anchored on Ni foam for efficient electrocatalytic water splitting and urea electrolysis, Chemical Engineering Journal, Chem. Eng. J. 390 (2020) 124525.

[61] J. Ma, P. S. Li, X. Lin , Y. J. Huang , Y. Zhong , L. P. Zhang, X. M. Sun, D. J. Zhou, W. F. Lin, Z. H. Xia, Electronic coupling strategy to boost water oxidation efficiency based on the modelling of trimetallic hydroxides $Ni_{1-x-y}Fe_xCr_y(OH)_2$: From theory to experiment, Chem. Eng. J. 402 (2020) 126144.

[62] Y. J. Lia, X. F. Zhou, Weihong Qi, H. P. Xie, K. Yin, Y. G. Tong, J. He, S. Gong, Z. Li, Ultrafast fabrication of Cu oxide micro/nano-structures via laser ablation to promote oxygen evolution reaction, Chem. Eng. J. 383 (2020) 123086

ToC Figure

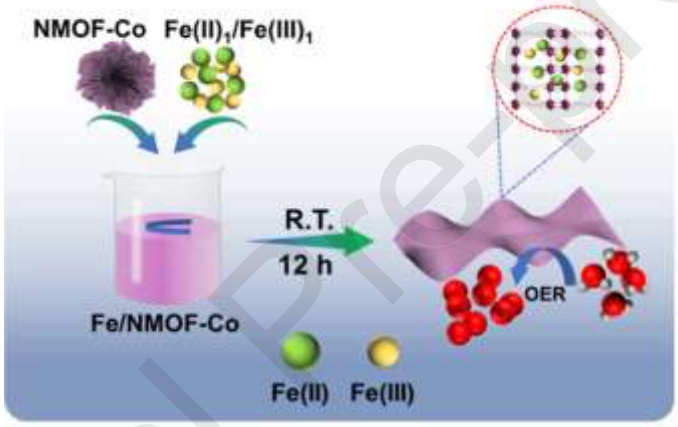

Fe-incorporated Co-based ultrathin metal-organic framework catalysts $(Fe(II)_1Fe(III)_1)_x$/NMOF-Co) exhibits superior oxygen evolution reaction (OER) catalytic performance, and shines the new light for the real application of free-noble metal catalysts in electrocatalysis.

HIGHLIGHTS

• Controlled molar ratios of Fe to NMOF-Co inside Co-based ultrathin nanosheets is designed.

• The ultrathin nanostructures provided extra active sites and enlarged active area.

• High OER activity is achieved due to large ECSA and optimized molar ratios of Fe to MOF nanosheets.

• The catalyst showed excellent catalytic activity and stability for OER.